Scalar flux in a uniform mean scalar gradient in homogeneous isotropic steady turbulence

Toshiyuki Gotoh[a,b,*], Takeshi Watanabe[a,b]

[a] *Graduate School of Engineering, Department of Scientific and Engineering Simulation, Nagoya Institute of Technology, Gokiso, Showa-ku, Nagoya, 466-8555, Japan*
[b] *CREST, Japan Science and Technology Agency, 4-1-8 Honcho, Kawaguchi, Saitama 332-0012, Japan*

Abstract

Statistics of a passive scalar flux in a uniform mean scalar gradient convected by homogeneous isotropic steady turbulence are numerically studied by using very high resolution direct numerical simulation. It is found that the Nusselt number increases in proportion to the Péclet number and that the one point probability density function of the scalar flux is negatively skewed exponential and insensitive to the variation of the Péclet number. The scalar field is studied by visualization and ramp-cliff structure and mesa-canyon structure are observed along the directions parallel and perpendicular to the mean scalar gradient, respectively. The probability density function of the scalar flux is theoretically computed and found to be in good agreement with the numerical results. A Lagrangian statistical theory for the scalar flux is developed and predicts that the scalar transfer flux is given by the time integral of the Lagrangian velocity autocorrelation and increases in proportion to the Péclet number which is consistent with the results of the direct numerical simulation. A physical explanation of the asymmetry of the scalar flux PDF is explored.

Keywords: Turbulence, Passive scalar, Scalar flux, Statistics, Nusselt number, Péclet number, Probability density function

1. Introduction

Transport of a scalar by turbulent flow is one of the central issues of fundamental physics of turbulence and important in engineering, oceanographic and atmospheric applications [1, 2, 3]. In many cases there exists a mean scalar gradient in turbulent flows which can be quite often regarded as uniform over the distances longer than the characteristic macro scale of the turbulent flows. When the mean scalar gradient is uniform, say in x_3 direction, the total scalar field is written as $\Theta = \Gamma x_3 + \theta$ where $\Gamma = \langle \nabla \Theta \rangle$ is the uniform mean scalar gradient, θ is the scalar fluctuation and $\langle\ \rangle$ is the ensemble average. In this circumstance, there exists a nonzero mean scalar flux $\overline{q} = \langle \theta u_3 \rangle$ along the direction of the mean gradient, where u_3 is the velocity component parallel to the mean scalar gradient. The nondimensional scalar flux is the Nusselt number which is defined by

$$Nu = -\frac{\langle \theta u_3 \rangle}{\kappa \Gamma}\ , \tag{1}$$

where κ is the molecular diffusivity of the passive scalar. It is known that Nu increases with the Péclet number but its prediction and evaluation as to how large and how fast it grows with respect to Péclet number and other turbulence characteristics are still not well understood [4, 5].

The scalar flux fluctuates around its mean value. Since the scalar flux is the product of the scalar and the velocity component along the mean gradient, one point probability density function (PDF) of the scalar flux is dependent on the statistics of the velocity and scalar or their joint PDF. It is well known that the one point PDF of the velocity is approximately Gaussian distribution, but there are arguments about the PDF of the passive scalar in turbulence, Gaussian or exponential. It has been argued that condition for observing the exponential tail of PDF of the scalar amplitudes is stringent and the system size needs to be large enough when compared to the integral scale of the turbulent velocity field [2, 4, 6, 7, 8, 9, 10]. There are many studies on the asymptotic behavior of the PDFs and/or the moments of the velocity and passive scalar at small scales, especially on the scaling properties from the view point of the uni-

*Corresponding author
Email addresses: gotoh.toshiyuki@nitech.ac.jp (Toshiyuki Gotoh), watanabe@nitech.ac.jp (Takeshi Watanabe)

versality [2, 3, 11, 12, 13, 14]. On the other hand, the fluctuations of the scalar have attracted less attention, in spite of their practical and fundamental importance. This seems partly due to the fact that the scalar flux is the quantity dominated by large scales of motion where universality is less expected. However, in order to understand the interplay between the velocity and scalar fields and to get better prediction of the scalar transport, it is necessary and indispensable to examine the flux fluctuations around the mean under an ideal circumstance. In this paper, we describe results of a series of direct numerical simulations (DNSs) of a passive scalar convected by isotropic steady turbulence under the uniform mean scalar gradient, and analyze the statistical behavior of the fluctuations of the scalar flux, especially, the Péclet number dependence of the Nusselt number and the one point PDF of the scalar flux. We also develop a statistical theory for the mean value and the PDF of the scalar flux and compare with the DNS results, and explore the physical explanation for the results.

2. Direct Numerical Simulation

The incompressible velocity field $u_i(\boldsymbol{x}, t)$ and the scalar field $\theta(\boldsymbol{x}, t)$ are assumed to be governed by the Navier-Stokes and advection-diffusion equations,

$$(\partial_t + u_j\partial_j)u_i = -\partial_i P + \nu\partial_j^2 u_i + f_i, \quad \partial_i u_i = 0, \quad (1a,b)$$

$$(\partial_t + u_j\partial_j)\theta = \kappa\partial_j^2\theta - \Gamma u_3, \quad (2)$$

respectively, where the summation convention over repeated indices is assumed. The external solenoidal Gaussian random force f_i which has spectrum support at low wavenumber band $1 \le |\boldsymbol{k}| \le 2$ is added to maintain a statistical steady state [15, 16]. Equations (1) and (2) were numerically integrated in a periodic box of size $\mathcal{L} = 2\pi$. Pseudo spectral method was used for the nonlinear and convective terms, and the time integration was performed by using the fourth-order Runge-Kutta-Gill method. The uniform mean scalar gradient was set to be $\Gamma = 1$ without loss of generality. The spectra of the kinetic energy and scalar variance, and the cospectrum of the scalar flux are defined by

$$E = \frac{1}{2}\left\langle \boldsymbol{u}^2 \right\rangle = \frac{3}{2}u'^2 = \int_0^\infty E(k)\,\mathrm{d}k, \quad (3)$$

$$E_\theta = \frac{1}{2}\left\langle \theta^2 \right\rangle = \frac{1}{2}\theta'^2 = \int_0^\infty E_\theta(k)\,\mathrm{d}k, \quad (4)$$

$$-\langle u_3\theta\rangle = \int_0^\infty E_{u\theta}(k)\,\mathrm{d}k, \quad (5)$$

respectively, where u' and θ' are the root mean squares of the velocity and scalar fluctuations. The angle bracket $\langle\cdots\rangle$ indicates the spatial and temporal averages. The mean dissipation rates for E and E_θ are defined by

$$\overline{\epsilon} = \frac{\nu}{2}\left\langle \left(\partial_i u_j + \partial_j u_i\right)^2 \right\rangle, \quad \overline{\chi} = \kappa\left\langle (\partial_i\theta)^2 \right\rangle, \quad (6a,b)$$

respectively, and we introduce several characteristic scales, such as the integral scales,

$$L = \frac{3\pi}{4E}\int_0^\infty k^{-1}E(k)\,\mathrm{d}k, \quad L_\theta = \frac{\pi}{2E_\theta}\int_0^\infty k^{-1}E_\theta(k)\,\mathrm{d}k, \quad (7a,b)$$

the Taylor microscales,

$$\lambda = \sqrt{\left\langle u_1^2 \right\rangle / \langle(\partial_1 u_1)^2\rangle}, \quad \lambda_\theta = \sqrt{\langle\theta^2\rangle / \langle(\partial_1\theta)^2\rangle}, \quad (8a,b)$$

the Kolmogorov and Batchelor scales,

$$\overline{\eta} = \left(\frac{\nu^3}{\overline{\epsilon}}\right)^{1/4}, \quad \overline{\eta}_B = \left(\frac{\kappa^2\nu}{\overline{\epsilon}}\right)^{1/4} = \overline{\eta}Sc^{-1/2}, \quad (9a,b)$$

and the skewness of the velocity and passive scalar

$$S(t) = \frac{\langle(\partial_1 u_1)^3\rangle}{\langle(\partial_1 u_1)^2\rangle^{3/2}}, \quad S_\theta(t) = \frac{\langle(\partial_1 u_1)(\partial_1\theta)^2\rangle}{\langle(\partial_1 u_1)^2\rangle^{1/2}\langle(\partial_1\theta)^2\rangle}, \quad (10a,b)$$

respectively. The correlation coefficient between the passive scalar and the velocity along the direction of the mean scalar gradient is defined by

$$r = \langle\theta u_3\rangle / \theta' u'. \quad (11)$$

A series of DNSs is characterized by the Péclet number $Pe = u'L/\kappa$, Taylor microscale Reynolds number $R_\lambda = u'\lambda/\nu$ and Schmidt number $Sc = \nu/\kappa$, and parameters of DNSs are listed in Table 1. Runs G1 to G4 are conducted to examine the Reynolds number effects with $Sc = 1$ and Runs S01 and S2 are made to see the Schmidt number effects with constant Reynolds numbers at about $R_\lambda = 174$. K_{max} is the maximum wavenumber retained in DNS and T_{av} is the time duration of the time average. Since the scalar flux is the large scale quantity, it is necessary to average over longer time interval to achieve good statistical convergence. As for the spatial resolution, an overall criterion for the accuracy in the spatial resolution is $K_{max}\eta > 1 \sim 2$ [11, 15, 17, 18, 19, 20]. Watanabe and Gotoh studied systematically the accuracy of the statistics obtained by DNS and found that the statistical data of low to moderate order at scales larger than the dissipation scale is

Table 1: DNS parameters.

Run	G1	G2	G3	G4	S01	S2
N^3	256^3	512^3	1024^3	2048^3	256^3	512^3
Re	973	2160	6480	10200	1000	933
Pe	973	2160	6480	10200	100	1870
R_λ	174	263	468	586	176	170
Sc	1	1	1	1	0.1	2
$\nu(\times 10^{-3})$	1.3	0.60	0.24	0.13	1.3	1.3
$K_{max}\overline{\eta}$	0.99	1.09	1.05	1.39	0.99	1.97
$T_{av}u'/L$	27.1	5.62	3.97	2.29	7.01	8.90
u'	1.07	1.10	1.21	1.11	1.07	1.06
θ'	1.61	1.58	1.88	1.22	1.78	1.46
L	1.18	1.17	1.28	1.19	1.21	1.14
L_θ	0.745	0.752	0.778	0.662	1.03	0.631
$\lambda(\times 10^{-1})$	2.12	1.44	0.927	0.686	2.15	2.09
$\lambda_\theta(\times 10^{-1})$	1.07	0.712	0.432	0.312	3.36	0.743
$-S_u$	0.508	0.530	0.559	0.610	0.505	0.545
$-S_\theta$	0.434	0.458	0.450	0.508	0.497	0.493
$\overline{\epsilon}L/u'^3$	0.482	0.468	0.444	0.446	0.486	0.484
$\overline{\chi}L/u'\theta'^2$	0.379	0.378	0.402	0.430	0.387	0.379
$\langle q\rangle$	−0.885	−0.919	−1.05	−0.599	−1.13	−0.698
σ_q	1.92	1.82	2.40	1.37	2.10	1.63
$r = \langle q\rangle/u'\theta'$	−0.517	−0.532	−0.460	−0.442	−0.598	−0.453
$\sigma_q/u'\theta'$	1.12	1.05	1.06	1.01	1.10	1.05
$Nu = q/\kappa\Gamma$	678	1530	4390	4700	87.1	1070
$\Gamma q/\overline{\chi}$	1.00	1.05	0.785	1.01	1.06	0.934
$A = \Gamma L/\theta'$	0.733	0.741	0.681	0.975	0.680	0.781

insensitive to the resolution provided that $K_{max}\overline{\eta} > 1$ [21]. Therefore we consider that the one point statistics of the velocity and scalar amplitudes and the spectrum at wavenumbers below the dissipation range in the present study do not suffer from the resolution effects.

It is important and useful to examine the statistical nature of the scalar injection $f_\theta(\boldsymbol{x}, t) \equiv -\Gamma u_3(\boldsymbol{x}, t)$ in Eq.(2). The statistics of f_θ is identical to that of u_3, so that f_θ is statistically steady, homogeneous and the one point statistics of f_θ is close to the Gaussian, and its Eulerian two point two time correlation is given by

$$\langle f_\theta(\boldsymbol{x}, t)\rangle = 0, \tag{12}$$

$$\langle f_\theta(\boldsymbol{x}+\boldsymbol{r}, t) f_\theta(\boldsymbol{x}, s)\rangle = \Gamma^2 u'^2 \left(\frac{1}{3r^2}\frac{d}{dr}(r^3 f) - \frac{r}{3}\frac{df(r)}{dr}P_2(\cos\phi)\right) \times G^E\left(u'|t-s|/r\right), \tag{13}$$

where ϕ is the angle between the direction of the mean scalar gradient and $\boldsymbol{r}$, and $f(r)$ is the longitudinal velocity correlation function. The function $G^E(x)$ describes the Eulerian decorrelation in time and monotonically decreasing function of x. Equation (13) means that the correlation function of the scalar injection has the anisotropic contributions from the $l = 2$ sector of the SO(3) decomposition, thus the scalar field is excited at all the wavenumbers up to k_d, which is in sharp contrast to the case of the random scalar injection which is applied only at low wavenumbers. Since the integral scale of the longitudinal velocity correlation functions is twice that of the transverse one as $L_\parallel = 2L_\perp$ at large scales and $\lambda_\parallel = \sqrt{2}\lambda_\perp$ at small scales, the same anisotropy as that of u_3 is imprinted on f_θ at all of the scales. Moreover, the source term shares the same correlation time and intermittency effects with those of u_3.

3. Spectra

The spectrum carries very fundamental knowledge about the distribution of the fluctuations over the scale. In this section we briefly describe the spectra of the kinetic energy and the scalar variance for completeness although they have already been published in [26]. The compensated spectra of the three dimensional kinetic energy $\overline{\epsilon}^{-2/3}k^{5/3}E(k)$ and scalar variance $\overline{\chi}^{-1}\overline{\epsilon}^{1/3}k^{5/3}E_\theta(k)$ are plotted in Figs. 1 and 2, respectively [27, 28, 29]. Since the scalar spectrum is weakly anisotropic, the three dimensional spectrum $E_\theta(k)$ is understood as the isotropic sector in the $SO(3)$ decom-

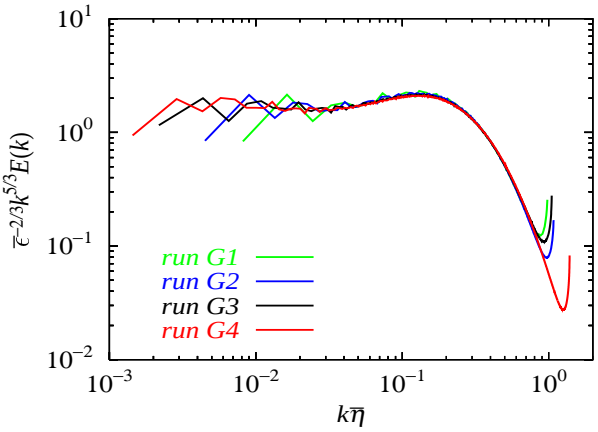

Figure 1: Compensated energy spectrum $\overline{\epsilon}^{-2/3}k^{5/3}E(k)$.

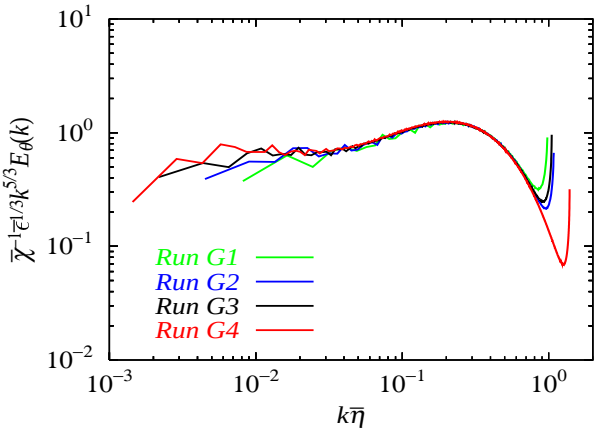

Figure 2: Compensated scalar variance spectrum $\overline{\chi}^{-1}\overline{\epsilon}^{1/3}k^{5/3}E_\theta(k)$.

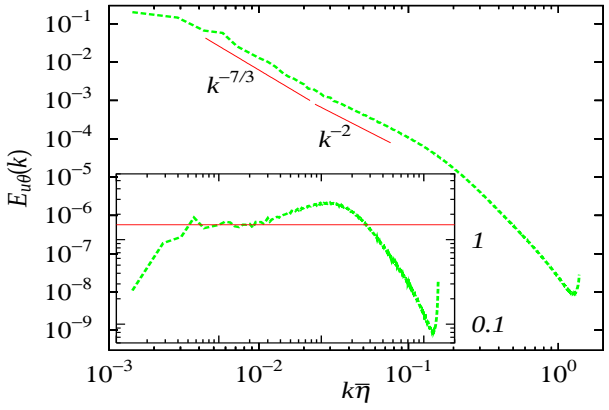

Figure 3: Three dimensional spectrum of scalar flux. Inset figure shows the compensated three dimensional spectrum $\Gamma^{-1}\overline{\epsilon}^{-1/3}k^{7/3}E_{u\theta}(k)$.

position. The Kolmogorov and Obukhov-Corrsin constants are found to be $K = 1.61$ and $K_{OC} = 0.68$, respectively which are in good agreement with those by DNSs [11, 12, 15, 16, 26, 30] and by the experiments [1, 31, 32]. Similarly Obukhov-Corrsin constant in the one dimensional scalar spectrum in x_3 direction is computed as $C_\theta^{1D} = 0.408$ which is close to the experimental values 0.4 [32] and $0.45 - 0.55$ [5, 22] and 0.4 by DNS [11].

The cospectrum of the scalar in three dimensions is shown in Fig. 3 and the compensated spectrum $\Gamma^{-1}\overline{\epsilon}^{-1/3}k^{7/3}E_{u\theta}(k)$ is plotted in the inset figure at $R_\lambda = 586$ [26]. There have been arguments about as to whether the scaling exponent of the scalar flux spectrum is -2 or $-7/3$ in the inertial range [5, 22]. A theoretical study using EDQNM [25] suggests a slow approach to $7/3$ only for very large R_λ. The present DNS data supports the Lumley scaling of $E_{u\theta}(k) \propto k^{-7/3}$ [23, 24]. One reason for the dispute is presumably due to the fact that the Reynolds numbers of the previous DNS studies were not high enough to achieve the well developed scaling range.

4. Field structure

It is interesting and useful to see the scalar field structure before going to the detailed analysis of the scalar flux. Figure 4 shows the total scalar (top) and the scalar dissipation fields (bottom) in the plane parallel to the uniform mean scalar gradient, respectively. In the plateau regions in Fig.4, the total scalar field is nearly constant with small fluctuations, which means that the scalar field is well mixed, and jumps at the periphery, forming a stair structure [1, 33, 34, 35]. The boundary formed by the jumps tends to align with the direction perpendicular to the mean gradient, and is highly convoluted (readers may enlarge the PDF version of the figures). The typical length of the sharp boundary is a few times the velocity integral scale. Also at the sharp jumps the scalar dissipation has large values as expected and seen in the bottom plate of Fig.4 [7, 12].

In order to see the field in more precisely, the velocity u_3, scalar θ (or total scalar $\Gamma x_3 + \theta$) and scalar flux $q = u_3\theta$ are plotted along the coordinate parallel and perpendicular to the mean scalar gradient for Run G3. Three bars in each figure show the integral scales of the velocity L, scalar L_θ and half the velocity integral scale $L/2$, respectively. In Fig.5(a), the scalar fluctuations have plateau regions and jumps, mesa-canyon structure along the x_1 direction. Although it is difficult to say which length scale L, L_θ, or $L/2$ is relevant, the

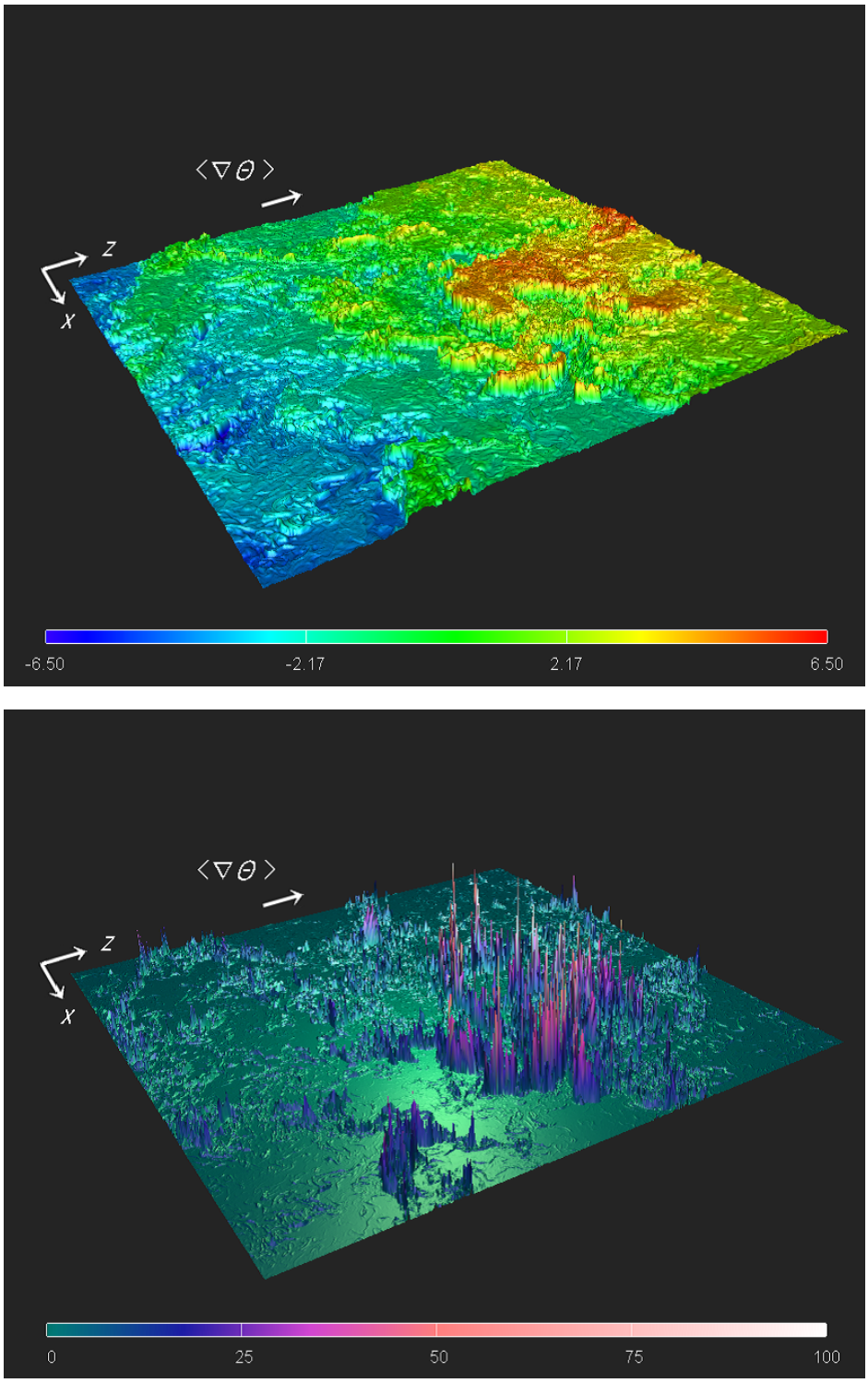

Figure 4: Total scalar amplitude (top) and the scalar dissipation (bottom) in (x, z) plane at $Pe = 6480$ of Run G3.

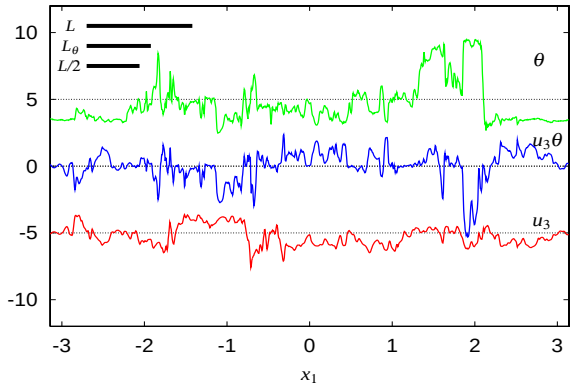

(a) Variation of θ (green), $q = u_3\theta$ (blue) and u_3 (red) with respect to x_1 at $(x_2 = -\pi, x_3 = 0)$.

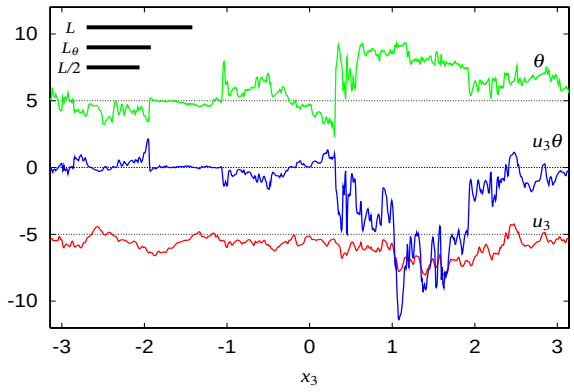

(b) Variation of θ (green), $q = u_3\theta$ (blue) and u_3 (red) with respect to x_3 at $(x_1 = 0, x_2 = -\pi)$.

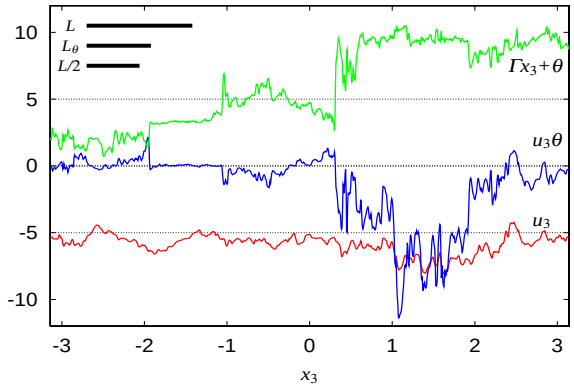

(c) Variation of $\Gamma x_3 + \theta$ (green), $q = u_3\theta$ (blue) and u_3 (red) with respect to x_3 at $(x_1 = 0, x_2 = -\pi)$.

Figure 5: One dimensional plots of the velocity u_3, scalar fluctuations, and scalar flux for Run G3. Curves of the velocity and scalar are shifted by -5 and 5, respectively, and black dotted lines show the zero level for each field. The black solid bars represent L for the longitudinal velocity correlation and L_θ the scalar correlation, and $L/2$ for the transversal velocity correlation, respectively.

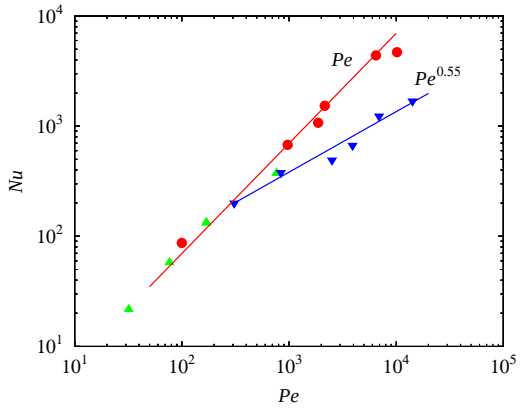

Figure 6: Variation of the Nusselt number against Péclet number. • (red) : present DNS, ▲ (green): DNS by Overholt and Pope [37], ▼ (blue): experiment by Mydlarski [5], Straight lines show $Nu \propto Pe$ for the theoretical prediction Eq.(33), and $Nu \propto Pe^{0.55}$ for the experiment, respectively.

characteristic length of the velocity u_3 along the x_1 direction looks to be closer to $L/2$ which is the integral scale of the transverse velocity, and the scalar fluctuations tend to have a similar length scale as inferred by the anisotropy of the scalar injection. On the other hand, the ramp-cliff structure is clearly seen in Fig.5(b) [1, 33, 34, 35, 36, 37]. Roughly speaking the signs of the velocity and scalar fluctuations are opposite, which is consistent with the negative value of the mean scalar flux. The jumps of the scalar amplitudes look to occur irrespective of the velocity fluctuation in this plot, and also appear as the magnified jumps in the scalar flux. Figure 5(c) shows that the total scalar has the wide plateau regions whose length is about L and the jumps, forming the stair structure. A common feature observed in the above plots is that the scalar fluctuations tend to have a large scale coherency (mesa-canyon and ramp-cliff structure) in the sense that the amplitudes of the scalar fluctuations are comparable to those of the small scale velocity over the velocity integral scale, and that the coherency is broken by the jumps whose strength are a few times the rms of the scalar fluctuations. This is a generic property of the passive scalar fluctuations and independent of the direction of the mean scalar gradient.

5. Statistics of scalar flux

Figure 6 shows the variation of the Nusselt number obtained by DNSs as well as those by experiment [5, 37] with respect to the Péclet number. The reason for plot-

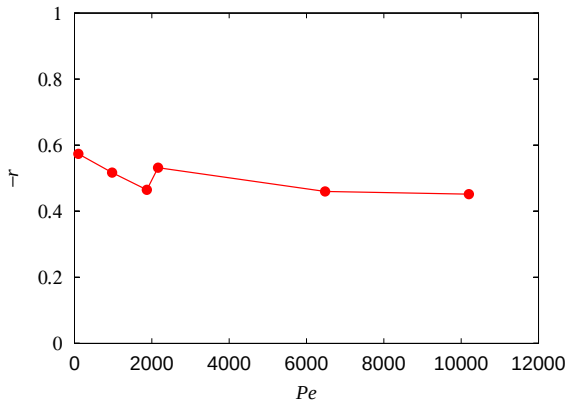

Figure 7: Variation of correlation coefficients against Péclet number.

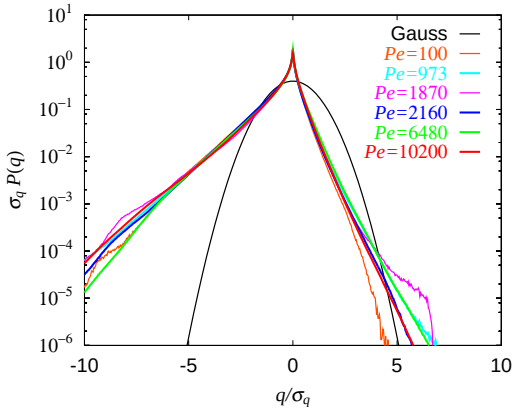

Figure 8: Normalized PDFs of scalar flux q/σ_q for various Péclet numbers.

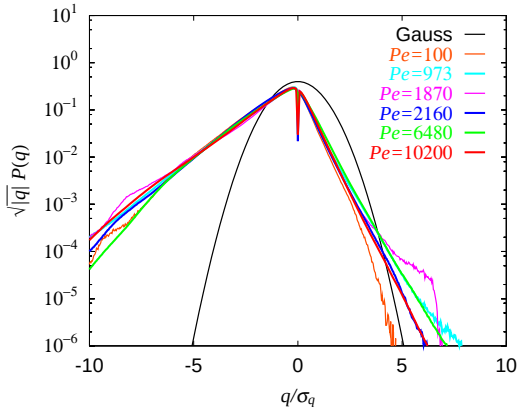

Figure 9: Normalized PDFs of scalar flux multiplied by $\sqrt{|q|}/\sigma_q$ for various Péclet numbers.

ting Nu against Pe instead of R_λ is due to the fact that the mean scalar flux $\langle\theta u_3\rangle$ is the quantity characterized by the large scale, which is also supported by the Lagrangian spectral theory predicting $Nu \propto Pe$ which will be described in Sec.6. The present DNS data and those by Overholt and Pope with $Pr = 0.7$ [37] scale well as $Nu \propto Pe$, the theoretical prediction. On the other hand, Nu by the experiments increases as $Nu \propto Pe^{0.88}$[4] or $Nu \propto Pe^{0.55}$[5] in which the exponents are evaluated by the least square fit. The reason for the slower increase is not known. The correlation coefficient r as a function of the Péclet number is also plotted in Fig.7. When the Péclet number is small, the correlation coefficient is weakly decreasing and approaches a constant about 0.45 for large Pe. Since the Nusselt number is given by Eq.(1), the nearly constant behavior of r is consistent with the scaling $Nu \propto Pe$.

Figure 8 shows the normalized PDFs $\sigma_q P(q)$ of the scalar flux for various Péclet numbers, where σ_q is the standard deviation of q. The PDF curves are well collapsed on a single curve and negatively skewed so that the left tails are longer than the right ones. The latter observation is consistent with the experimental observation by Mydlarski [5], while the skewness of the PDFs by DNS is slightly larger than in the experiments. The PDF curves for small $|q|$ are of the form of cusp of $|q|^{-1/2}$ which is predicted by the theory in Sec.6, and the cusp can be removed by multiplying $P(q)$ the prefactor $|q|^{1/2}$. Figure 9 shows the thus compensated PDFs which are straight lines and again well collapsed each other, meaning that the PDF $P(q)$ is exponential. The slope $c_\pm$ of the PDF defined by $P(q) \propto \exp(-c_\pm|q|/\sigma_q)$ for the positive and negative tails are computed by using the least square fit for the range of $-5 \le q \le -0.5$ and $0.5 \le q \le 2.0$, respectively and plotted in Fig.10. Both c_+ and c_- are almost constant over the range of the Péclet numbers studied.

We now theoretically consider the PDF of the scalar flux. Equation (2) means that in the steady state the passive scalar fluctuations are injected by the x_3 component of the turbulence velocity and thus θ and $w = u_3$ is well correlated. We assume that the one point PDFs of the velocity and scalar at large scales are close to the Gaussian, then it is reasonable to expect that θ and u_3 obey the joint Gaussian PDF as Thoroddsen and Van Atta studied [5, 38, 39]. We follow their approach in the following.

First we examine the one point PDFs of the velocity and scalar in Figs.11 and 12 by using DNS data. The normalized PDF of the velocity is approximately Gaussian, while that of the passive scalar decreases faster than the Gaussian and the curves are smooth over the range of unity to 10^{-6} [7]. Therefore we believe that the

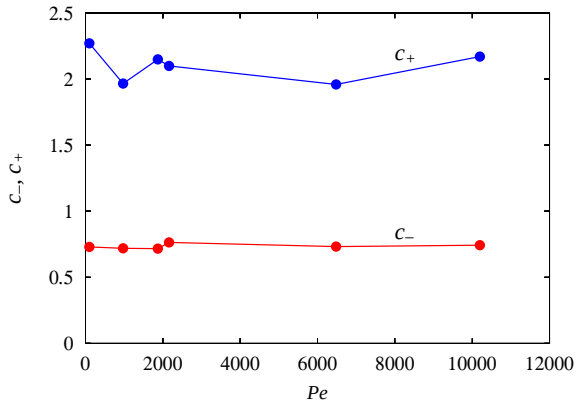

Figure 10: Variation of slope of the exponential PDFs of scalar flux against Péclet number.

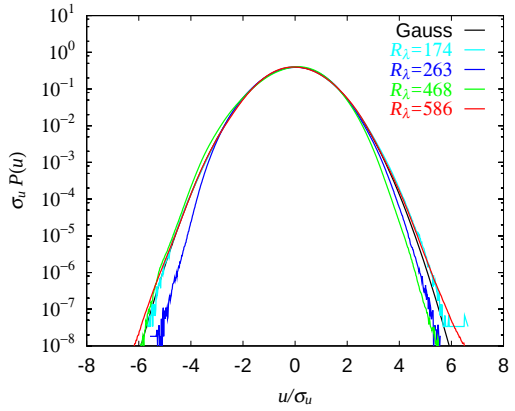

Figure 11: Normalized PDFs of velocity for various Reynolds numbers.

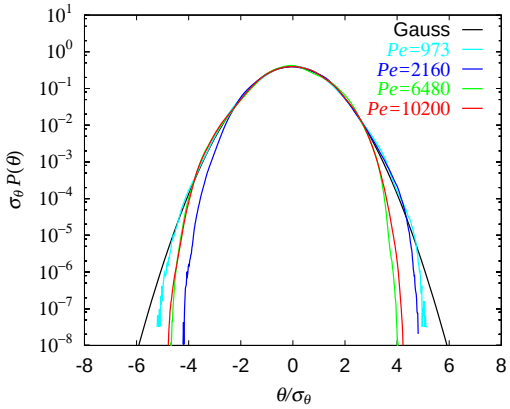

Figure 12: Normalized PDFs of scalar for various Péclet numbers.

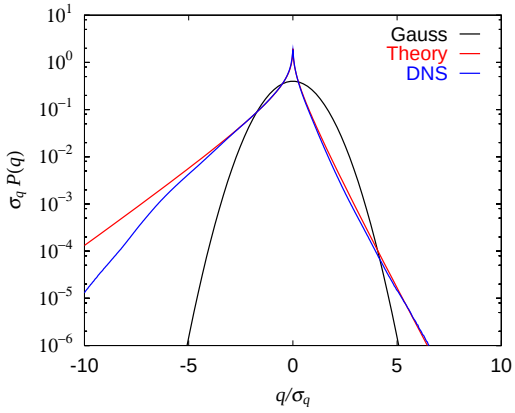

Figure 13: Comparison of theoretical prediction for PDF of scalar flux with DNS data at Pe = 6480.

faster decrease of $P(\theta)$ than the Gaussian is not due to the artifact of insufficient number of sample sizes.

With these observations of the PDFs of the velocity and scalar, we consider the joint PDF as

$$P(w,\theta)dwd\theta = \frac{1}{2\pi\sigma_w\sigma_\theta\sqrt{1-r^2}} \times \exp\left(-\frac{1}{2(1-r^2)}\left(\frac{w^2}{\sigma_w^2} - \frac{2rw\theta}{\sigma_w\sigma_\theta} + \frac{\theta^2}{\sigma_\theta^2}\right)\right)dwd\theta, \tag{14}$$

where $r = \langle w\theta\rangle \,/\, \sigma_w\sigma_\theta$. By changing the variables from (w,θ) to $(w, q = w\theta)$ and integrating over w we obtain

$$P(q)dq = \frac{1}{\pi\sigma_w\sigma_\theta\sqrt{1-r^2}}\exp\left(\frac{rq}{(1-r^2)\sigma_w\sigma_\theta}\right) \times K_0\left(\frac{|q|}{(1-r^2)\sigma_w\sigma_\theta}\right)dq, \tag{15}$$

where $K_0(x)$ is the modified Bessel function of the second kind at zeroth order. Since the asymptotic expression of $K_0(x)$ is $\sqrt{\frac{\pi}{2x}}e^{-x}$, we have the asymptotic form of the PDF of the scalar flux as

$$P(q) \sim \frac{1}{\sqrt{|q|}}\exp\left(-c_\pm\frac{|q|}{\sigma_q}\right), \quad c_\pm = \frac{1}{1\pm r}\left(\frac{\sigma_q}{\sigma_w\sigma_\theta}\right). \tag{16}$$

Equation (16) indicates that $P(q)$ has the prefactor $|q|^{-1/2}$ for small $|q|$ and is exponential for large $|q|$ with different slope for each side. Since $r < 0$, we have $c_- < c_+$ so that the left tail of PDF is higher than the right tail.

Figure 13 shows the comparison of the theoretical prediction Eq.(15) with the PDF obtained by DNS at Pe = 6480, in which the DNS data of the correlation coefficient r is substituted into Eq.(15). The theoretical PDF of the scalar flux agrees well with that by DNS except the far left tail, and the same trend is observed for

other Péclet numbers (figure not shown). The faster roll off of the left tail at large $|q|$ than the exponential may be attributed to the fact that the one point PDF of the passive scalar decreases faster than the Gaussian at the large amplitudes as seen in Fig.12, although the reason for the sub-Gaussian nature of the PDFs of the passive scalar is not well known.

6. Theory of scalar flux

We consider the scalar flux from the view point of the Lagrangian frame. For this purpose we introduce a set of Lagrangian variables. First, we define Lagrangian position $\boldsymbol{Z}(\boldsymbol{x}, s|t)$ as the position of a fluid particle measured at time t whose trajectory passes $\boldsymbol{x}$ at time s. Then a generalized Lagrangian velocity $\boldsymbol{v}(\boldsymbol{x}, s|t)$ is defined as the velocity measured at time t of the fluid particle, and a generalized Lagrangian scalar field $\theta(\boldsymbol{x}, s|t)$ is similarly defined as the amount of scalar carried by that fluid particle measured at time t (see Kraichnan 1965, Kaneda and Gotoh 1986). They satisfy

$$\frac{\partial \boldsymbol{Z}(\boldsymbol{x}, s|t)}{\partial t} = \boldsymbol{v}(\boldsymbol{x}, s|t) = \boldsymbol{u}(\boldsymbol{Z}(\boldsymbol{x}, s|t), t), \tag{17}$$

$$\theta(\boldsymbol{x}, s|t) = \theta(\boldsymbol{Z}(\boldsymbol{x}, s|t), t). \tag{18}$$

Note that $\boldsymbol{v}(\boldsymbol{x}, t|t) = \boldsymbol{u}(\boldsymbol{x}, t)$ and $\theta(\boldsymbol{x}, t|t) = \theta(\boldsymbol{x}, t)$. The Lagrangian position function is defined by

$$\psi(\boldsymbol{y}, t|\boldsymbol{x}, s) = \delta(\boldsymbol{y} - \boldsymbol{Z}(\boldsymbol{x}, s|t)) \tag{19}$$

and obeys the equation

$$\left(\frac{\partial}{\partial t} + \boldsymbol{u}(\boldsymbol{y}, t) \cdot \nabla_y\right)\psi(\boldsymbol{y}, t|\boldsymbol{x}, s) = 0, \tag{20}$$

$$\psi(\boldsymbol{y}, t|\boldsymbol{x}, t) = \delta(\boldsymbol{y} - \boldsymbol{x}), \tag{21}$$

where $\delta(\boldsymbol{x})$ is Dirac's delta function. Both generalized velocity and scalar are expressed in terms of the Lagrangian position function as

$$\boldsymbol{v}(\boldsymbol{x}, s|t) = \int \psi(\boldsymbol{y}, t|\boldsymbol{x}, s)\boldsymbol{u}(\boldsymbol{y}, t)\, \mathrm{d}\boldsymbol{y}, \tag{22}$$

$$\theta(\boldsymbol{x}, s|t) = \int \psi(\boldsymbol{y}, t|\boldsymbol{x}, s)\theta(\boldsymbol{y}, t)\, \mathrm{d}\boldsymbol{y}. \tag{23}$$

The equation of the generalized scalar field with respect to *measuring time* is obtained by differentiating $\theta(\boldsymbol{x}, s|t)$ by t, by using equation of ψ and θ, and by using the incompressibility condition for the velocity $\boldsymbol{u}$ as

$$\frac{D\theta(\boldsymbol{x}, s|t)}{Dt} = \int \psi(\boldsymbol{y}, t|\boldsymbol{x}, s)\left(\kappa\nabla_y^2\theta(\boldsymbol{y}, t) - \Gamma u_3(\boldsymbol{y}, t)\right)\, \mathrm{d}\boldsymbol{y}. \tag{24}$$

For the moment we neglect the molecular diffusion effects. Then the above equation can be integrated with respect to time t from the *initial time* s as

$$\theta(\boldsymbol{x}, s|t) = \theta(\boldsymbol{x}, s|s) - \Gamma\int_s^t v_3(\boldsymbol{x}, s|t')\, \mathrm{d}t' \tag{25}$$

$$= \theta(\boldsymbol{x}, s) - \Gamma\Delta Z_3(\boldsymbol{x}, s|t), \tag{26}$$

where $\Delta Z_3(\boldsymbol{x}, s|t) = Z_3(\boldsymbol{x}, s|t) - x_3$ is a displacement in x_3 direction of the fluid particle during the time interval $t - s$.

The above Eq.(26) suggests a mechanism to generate the ramp structure of the scalar fluctuations. Consider a set of times $s_j = s + j(t - s)/n, (j = 0, 1, \cdots n)$ and the $n + 1$ fluid particles that leave $\boldsymbol{x}$ at time s_j and arrive at $\boldsymbol{Z}(\boldsymbol{x}, s_j|t)$ at time t. Then those fluid particles are on a smooth curve (streak line) connecting the points $\boldsymbol{x}$ and $\boldsymbol{z} \equiv \boldsymbol{Z}(\boldsymbol{x}, s|t)$ and the scalar distribution on the curve is given by Eq.(26). Since the velocity component at scale of L varies slowly in time of the order of $T = L/u'$, the streak line formed by the set of fluid particles is approximately straight line with length of the order of $u'(t - s)$ provided that $t - s < T$, so that the distribution of the passive scalar is approximately a linear function of the local coordinate z, the ramp structure of the scalar fluctuations.

Let us consider the physical reason for the negatively skewed PDF of the scalar flux. When $\kappa = 0$, the equation (26) is also written as

$$\theta(\boldsymbol{x}, t|s) = \theta(\boldsymbol{x}, t|t) - \Gamma\int_t^s v_3(\boldsymbol{x}, t|t')\, \mathrm{d}t' \tag{27}$$

$$= \theta(\boldsymbol{x}, t) + \Gamma\Delta Z_3(\boldsymbol{x}, t|s), \quad \text{for } t \geq s \tag{28}$$

where $\Delta Z_3(\boldsymbol{x}, t|s) = x_3 - Z_3(\boldsymbol{x}, t|s)$ is the displacement in x_3 component during the time interval $t - s$. Suppose that the *initial* value of θ at time $s(\leq t)$ is zero, then the above equation means

$$\theta(\boldsymbol{x}, t) = -\Gamma\Delta Z_3(\boldsymbol{x}, t|s), \tag{29}$$

and the scalar flux is written as

$$\tilde{q}(\boldsymbol{x}, t) = -\Gamma u_3(\boldsymbol{x}, t)\Delta Z_3(\boldsymbol{x}, t|s) \quad \text{for } t \geq s \tag{30}$$

for the zero diffusivity. Negative $\tilde{q}$ occurs when u_3 and ΔZ_3 have the same sign. In other words, the fluid particle u_3 keeps moving in the same mode as before (see Fig.14). On the other hand, positive $\tilde{q}$ occurs when the signs of u_3 and ΔZ_3 are opposite, meaning that the fluid particle has changed its direction of motion in x_3 direction, and the x_3 component of the fluid velocity has changed its sign, at least one time. This turn of the fluid

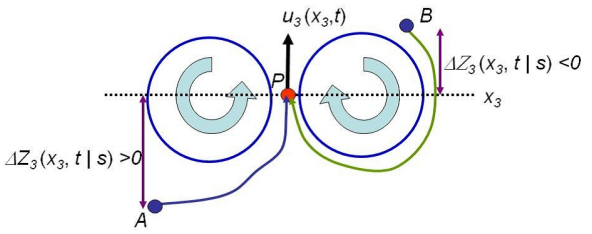

Figure 14: A schematic picture of the velocity and fluid particle excursion in the x_3 direction. For the path AP, $\Delta x_3(\boldsymbol{x}, t|s) > 0$ and $\tilde{q}_- = -\Gamma u_3(x_3, t)\Delta x_3(\boldsymbol{x}, t|s) < 0$. For the path BP, $\Delta x_3(\boldsymbol{x}, t|s) < 0$ and $\tilde{q}_+ = -\Gamma u_3(x_3, t)\Delta x_3(\boldsymbol{x}, t|s) > 0$. In order for the positive $\tilde{q}_+$ to be realized the fluid particle must turn before arriving at the position x_3, so that there is less chance for $\tilde{q}$ to have large positive values than in the case of the large negative $\tilde{q}$.

particle leads to the fact that the fluid particle experiences less chances of simultaneously having large velocity and large excursion ΔZ_3 with opposite sign, implying less probability of finding large positive scalar flux than in the negative one, thus we have $c_- < c_+$.

Now we consider the correlation between the velocity and scalar. We assume that the velocity and scalar fluctuations are statistically homogeneous, isotropic and in the steady state and $\kappa = 0$, then we proceed as

$$\begin{aligned}
\langle\theta(\boldsymbol{z},t)u_3(\boldsymbol{z},t)\rangle &= \langle\theta(\boldsymbol{Z}(\boldsymbol{x},s|t),t)u_3(\boldsymbol{Z}(\boldsymbol{x},s|t),t)\rangle \\
&= -\Gamma\int_s^t \langle v_3(\boldsymbol{x},s|t')v_3(\boldsymbol{x},s|t)\rangle\,\mathrm{d}t' \\
&\qquad +\langle\theta(\boldsymbol{x},s)u_3(\boldsymbol{Z}(\boldsymbol{x},s|t),t)\rangle \\
&= -\Gamma\int_s^t \langle v_3(\boldsymbol{x},s|t')v_3(\boldsymbol{x},s|t)\rangle\,\mathrm{d}t' \\
&= -\frac{\Gamma}{V}\int_s^t\int \langle v_3(\boldsymbol{x},s|t')v_3(\boldsymbol{x},s|t)\rangle\,\mathrm{d}\boldsymbol{x}\,\mathrm{d}t' \\
&= -\frac{\Gamma}{V}\int_s^t\int \langle v_3(\boldsymbol{x},t'|t')v_3(\boldsymbol{x},t'|t)\rangle\,\mathrm{d}\boldsymbol{x}\,\mathrm{d}t' \\
&= -\Gamma\int_s^t Q_{33}^L(\boldsymbol{x},t'|t)\,\mathrm{d}t' < 0, \qquad (31)
\end{aligned}$$

where $Q_{33}^L(\boldsymbol{x},t'|t)$ is the autocorrelation function of the Lagrangian velocity in the x_3 direction. The first line is due to the homogeneity, stationarity, and zero diffusivity, the passage from the second to the third line uses the fact that the velocity at time $t > s$ is independent of the passive scalar, the fourth line is due to the homogeneity, the fifth line is obtained by using the labeling time transformation for the homogeneous system ([40, 41, 42]). Equation (31) shows that the correlation $\langle\theta u_3\rangle$ is given by the time integral of the Lagrangian autocorrelation of the velocity in the direction parallel to the mean scalar gradient. Since the velocity field is isotropic and in steady state, we may write as

$$\langle\theta(\boldsymbol{z},t)u_3(\boldsymbol{z},t)\rangle = -\frac{\Gamma}{3}\int_0^\infty Q^L(t')\,\mathrm{d}t' = -C_q\Gamma u' L, \quad (32)$$

where $Q^L(t) = \langle\boldsymbol{v}(\boldsymbol{x},0|t)\cdot\boldsymbol{v}(\boldsymbol{x},0|0)\rangle$, T_L is the Lagrangian integral time of the velocity autocorrelation and C_q is a nondimensional constant of the order one. Therefore the Nusselt number is computed as

$$N_u = -\frac{\langle\theta u_3\rangle}{\kappa\Gamma} = -C_q Pe \sim C_q Sc R_\lambda^2. \qquad (33)$$

If we substitute the relation $Re \propto Ra^{1/2}Sc^{-1/2}$ into Eq.(33), we have $Nu \propto (RaSc)^{1/2}$ for the moderate Sc which corresponds to the Kraichnan regime [43]. Equation (33) is consistent with DNS data as seen in Fig.1.

The correlation r is estimated as

$$r = \frac{\langle w\theta\rangle}{\sigma_w\sigma_\theta} = \frac{\kappa\Gamma}{\sigma_w\sigma_\theta}\frac{\langle w\theta\rangle}{\kappa\Gamma} = -A\frac{Nu}{Pe} = -AC_q, \qquad (34)$$

$$A = -\frac{\Gamma L}{\sigma_\theta} \qquad (35)$$

where A is the nondimensional constant of the order unity and listed in Table 1. The correlation is independent of Pe in the limit of large Péclet number, which agrees well with the DNS results in Fig.7.

The constant C_q can be evaluated in the large Péclet number limit by using the Lagrangian renormalized approximation (LRA) which is a Lagrangian spectral theory developed by Kaneda [44, 45]. The result is

$$C_q = \frac{1}{2}K^{1/2}I \approx 0.734, \quad I = \int_0^\infty G^L(x)dx = 1.2, \quad (36)$$

where $K = 1.72$ is the Kolmogorov constant computed by LRA and G^L is the Lagrangian response function. When the value A is read from Table 1, we have $-r = AC_q = 0.500$ for Run G3 which is close to the DNS value as seen in Fig.7.

7. Summary

We have studied the passive scalar flux convected by homogeneous isotropic steady turbulence under the uniform mean scalar gradient by using the very high resolution DNSs. It was found that the isotropic sector of the scalar spectrum has the small but finite width of the inertial-convective range with the exponent close to $-5/3$ and the cospectrum has the exponent $-7/3$. The Nusselt number was found to scale as $Nu \propto Pe$. The field structures of the scalar, total scalar and scalar dissipation were visualized and it was observed that the stair

structure for the total scalar and the mesa-canyon structure for the scalar in the direction parallel and perpendicular to the mean gradient, respectively. Large scale coherent structure within which there exist small amplitude fluctuations and sharp jumps at periphery are generic feature of the passive scalar field convected by turbulence. The PDF of the scalar flux was also computed and compared with the theoretical prediction starting from the joint Gaussian PDF for the velocity and scalar. It was found that the PDFs are negatively skewed and exponential with the prefactor $|q|^{-1/2}$ and very insensitive to the Péclet number. The rates of roll off of the PDFs were computed by the joint Gaussian theory and found to be expressed in terms of the correlation coefficient between the velocity and scalar at large scales. The Lagrangian theory for the mean scalar flux (the Nusselt number) was developed for the zero limit of the diffusivity and found to be $Nu \propto Pe$ which agrees well with the DNS data. The ramp structure was explained by the Lagrangian theory. It was shown that the asymmetry of the PDF of the scalar flux is interpreted as the way that the fluid motion with the same sign in the velocity and displacement of a fluid particle is more probable than the one with opposite sign.

Acknowledgment

T. Gotoh thanks Prof. Antonia, Dr. Rubinstein, Profs. Sawford, Sreenivasan, Vassilicos, and Warhaft, for their valuable discussions and comments. We thank the Theory and Computer Simulation Center of the National Institute for Fusion Science (NIFS10KTAS006), the Information Technology Center of Nagoya University, and JHPCN for providing the computational resources. The authors thank Mr.Suzuki for his assistance in making computer graphics. T.G. and T.W's work were partially supported by Grant-in-Aid for Scientific Research No. 21360082 and No. 20760112 respectively, from the Ministry of Education, Culture, Sports, Science and Technology of Japan.

References

[1] K. R. Sreenivasan, 434 Proc. Roy. Soc. Lond A (1991) 165–182.
[2] Z. Warhaft, 32 Ann. Rev. Fluid Mech. (2000) 203–240.
[3] B. I. Shraiman, E. D. Siggia, 405 Nature (2000) 639–646.
[4] Jayesh, Z. Warhaft, A4 Phys. Fluids (1992) 2292–2306.
[5] L. Mydlarski, 475, J. Fluid Mech. (2003) 173–203.
[6] Jayesh, Z. Warhaft, 16 Phys. Rev. Lett. (1991) 3503–3506.
[7] P. Kailasnath, K. R. Sreenivasan, J. R. Saylor, 5 Phys. Fluids A (1993) 3207–3215.
[8] M. Ferchichi, S. Tavoularis, 461 J. Fluid Mech. (2002) 155–182.
[9] A. Pumir, B. Shraiman, E. D. Siggia 66 Phys. Rev. Lett. (1991) 2984–2987.
[10] B. I. Shraiman, E. D. Siggia, 49 Phys. Rev. E, (1994) 2912–2927.
[11] P. K. Yeung, S. Xu, K. R. Sreenivasan, 14 Phys. Fluids (2002) 4178–4191.
[12] P. K. Yeung, D. A. Donzis, K. R. Sreenivasan, 17, Phys. Fluids (2005) 081703 (4 pages).
[13] J. Schumacher, K. R. Sreenivasan, P. K. Yeung, 531 J. Fluid Mech. (2005) 113–122.
[14] T. Watanabe, T. Gotoh, 18, Phys. Fluids (2006) 058105 (4 pages).
[15] T Gotoh, D. Fukayama, T. Nakano, 14 Phys. Fluids (2002) 1065–1081.
[16] T. Watanabe, T. Gotoh, 6 New J. Phys. (2004) 40 (36 pages).
[17] V. Eswaran, S. B. Pope, 31, Phys. Fluids (1988) 506–520.
[18] L. P. Wang, S. Y. Chen, J. G. Brasseur, 400 J. Fluid Mech. (1999) 163–197.
[19] Y. Kaneda, T. Ishihara, M. Yokokawa, T. Itakura, A. Uno, 15 Phys. Fluids (2003) L21–L24.
[20] K. R. Sreenivasan, 72, Flow Turb. Combust. (2004) 115–141.
[21] T. Watanabe, T. Gotoh, 590 J. Fluid Mech. (2007*a*) 117-146.
[22] L. Mydlarski, Z. Warhaft, 358 J. Fluid Mech. (1998) 135–175.
[23] 21, J. Atmos. Sci., (1964) 99–102.
[24] J. L., Lumley, 10 Phys. Fluids, (1967) 855–858.
[25] W. J. T., Bos, H. Touil, J.-P. Bertoglio, 17 Phys. Fluids, 17, (2005) 125108 (8 pages).
[26] T. Watanabe, T. Gotoh, 19 Phys. Fluids (2007*b*) 121701.
[27] A. N. Kolmogorov, 30 C. R. Acad. Sci. USSR (1941) 301–305.
[28] A. M. Obukhov, 13 Isv. Geogr. Geophys. Ser. (1949) 58–69.
[29] S. Corrsin, 22 J. Appl. Phys. (1951) 469–473.
[30] T. Ishihara, T. Gotoh, Y. Kaneda, 41 Ann. Rev. Fluid Mech. (2009) 165–180.
[31] K. R. Sreenivasan, 7 Phys. Fluids (1995) 2778–2284
[32] K. R. Sreenivasan, 8 Phys. Fluids (1996) 189-196.
[33] A. Pumir, 6 Phys. Fluids (1994) 211–2132.
[34] M. Holzer, E. D. Siggia 6 Phys. Fluids (1994) 1820–1837.
[35] A. Celani, A. Lanotte, A. Mazzino, M. Vergassola, 13 Phys. Fluids (2001) 1768–1783.
[36] K. R. Sreenivasan, R. A. Antonia, D. Britz, 94 J. Fluid Mech. (1994)745–775.
[37] M. R. Overholt, S. B. Pope, 8 Phys. Fluids (1996) 3128–3148.
[38] S. T. Thoroddsen, C. W. Van Atta, 244 J. Fluid Mech. (1992) 547–566.
[39] S. Tavoularis, S. Corrsin 104 J. Fluid Mech. (1981) 311–347.
[40] R. H. Kraichnan, 8 Phys. Fluids (1965) 575–598.
[41] Y. Kaneda, T. Gotoh, A3 Phys. Fluids (1991) 1924–1933.
[42] T. Gotoh, R. S. Rogallo, J. R. Herring, R. H. Kraichnan, A5 Phys. Fluids (1993) 2846–2864.
[43] S. Grossmann, D. Lohse 407 J. Fluid Mech. (2000) 27–56.
[44] Y. Kaneda, 107 J. Fluid Mech. (1981) 131–146.
[45] Y. Kaneda, 29 Phys. Fluids (1986) 701–708.